

Article

Role of YSZ Particles on Microstructural, Wear, and Corrosion Behavior of Al-15%Mg₂Si Hybrid Composite for Marine Applications

Hamidreza Ghandvar ^{1,*}, Mostafa Abbas Jabbar ² , Michal Petrů ³ , Tuty Asma Abu Bakar ^{4,*}, Lim Jia Ler ⁴ and Seyed Saeid Rahimian Koloor ^{5,6,*} 

- ¹ Department of Chemical and Materials Engineering, New Uzbekistan University, Mastaqillik Ave. 54, Tashkent 100007, Uzbekistan
 - ² Department of Mechanical Techniques, Al-Nasiriya Technical Institute, Southern Technical University, Thi-Qar, Al-Nasiriya 64001, Iraq
 - ³ Faculty of Mechanical Engineering, Technical University of Liberec (TUL), Studentská 1402/2, 46117 Liberec, Czech Republic
 - ⁴ Faculty of Mechanical Engineering, Universiti Teknologi Malaysia, Johor Bahru 81310, Johor, Malaysia
 - ⁵ Institute for Nanomaterials, Advanced Technologies and Innovation (CXI), Technical University of Liberec (TUL), Studentská 1402/2, 46001 Liberec, Czech Republic
 - ⁶ Institute for Structural Engineering, Department of Civil Engineering and Environmental Sciences, Universität der Bundeswehr München, Werner-Heisenberg-Weg 39, Neubiberg, 85579 Munich, Germany
- * Correspondence: hgandvar@yahoo.com (H.G.); tuty@utm.my (T.A.A.B.); seyed.rahimian@tul.cz (S.S.R.K.)

Abstract: This study aims to investigate the microstructural alterations, mechanical properties, sliding wear behavior, and corrosion properties of Al-15%Mg₂Si composites with different contents of yttria-stabilized zirconia (YSZ). Al-15%Mg₂Si composites with the different contents of YSZ (0, 3, 6, and 9 wt.%) were fabricated using the stir-casting technique. The fabricated composites were characterized by means of optical microscopy (OM), scanning electron microscopy (SEM) equipped with energy-dispersive spectroscopy (EDS), Vickers hardness tester, linear reciprocating tribometer (LRT), and electrochemical test. The results showed that with the introduction of YSZ particles, the average size of the primary Mg₂Si particles in the base composite was 137.78 μm, which was reduced to 88.36 μm after adding 9 wt.% YSZ. The aspect ratio of Mg₂Si particles also decreased from 3, for the base composite, to 1.27 in the composite containing 9 wt.% YSZ. Moreover, the hardness value displays an incremental trend from 102.72 HV, as recorded for the base in situ composite, to 126.44 HV in the composite with 9 wt.% YSZ. On top of that, the Al-15%Mg₂Si-9%YSZ demonstrates exceptional wear resistance, with the lowest wear rate of 0.46 mm³/km under a 25 N applied load. Its average coefficient of friction (COF) was recorded at 0.42, which is lower than both the 3 and 6 wt.% of YSZ-containing composites. The smoother worn surface in Al-15%Mg₂Si-9%YSZ hybrid composite implies the abrasion phenomenon, as dominant wear behavior is milder than the other fabricated composites. On top of that, the Al-15%Mg₂Si-9%YSZ also possesses optimum corrosion resistance. The corrosion rate is 0.080 mmpy, comparable to the 0.164 mmpy rate obtained in the in situ composite.

Keywords: marine application; Al hybrid composites; Mg₂Si; YSZ; mechanical property; wear behavior; corrosion



Citation: Ghandvar, H.; Jabbar, M.A.; Petrů, M.; Bakar, T.A.A.; Ler, L.J.; Rahimian Koloor, S.S. Role of YSZ Particles on Microstructural, Wear, and Corrosion Behavior of Al-15%Mg₂Si Hybrid Composite for Marine Applications. *J. Mar. Sci. Eng.* **2023**, *11*, 1050. <https://doi.org/10.3390/jmse11051050>

Academic Editor: Erkan Oterkus

Received: 17 February 2023

Revised: 26 April 2023

Accepted: 4 May 2023

Published: 15 May 2023



Copyright: © 2023 by the authors. Licensee MDPI, Basel, Switzerland. This article is an open access article distributed under the terms and conditions of the Creative Commons Attribution (CC BY) license (<https://creativecommons.org/licenses/by/4.0/>).

1. Introduction

The use of various composite materials with metal [1], polymeric [2], or brittle [3] matrixes is highlighted in the mechanical design of structures in advanced industrial applications, such as aerospace, automotive, construction, and marine applications [4]. Composite materials are widely used in the marine industry due to their unique mechanical and corrosion properties [5]. Marine transport is increasing its usage of composites by

exploiting their two leading qualities: lightness and corrosion resistance. In this regard, the composite materials can be used as hull materials for naval warships [6], gratings, ducts, shafts, piping, hull shells [7], ferrocement for the development of low-cost barges/ferro boats, glass-reinforced plastic boats [5], sailboats, furniture on super-yachts and ocean racing applications [8]. Among the many types of composites [9], aluminum metal matrix composites (Al MMCs) are produced to have high specific strength and stiffness, suitable for many long-term energy-saving applications that aim to reduce the structures' weight in many industries, including robotics, rotating shafts, and automotive engine, and shipbuilding [10]. Al MMCs are generally produced with pure aluminum or aluminum alloys as their matrix materials. Due to their unique properties, such as a light weight, high specific strength, reasonable wear and corrosion resistance, controlled coefficient of thermal expansion, and high, good elevated-temperature stability, they are widely used in automobile and aerospace industries in the design of parts for advanced applications [11,12]. The density of aluminum alloys is nearly the same as the density of pure aluminum, which is approximately 2698 kg/m^3 . By incorporating aluminum into the production of MMC, the melting point increases significantly compared to the melting point of pure aluminum, which is $660 \text{ }^\circ\text{C}$. Pure aluminum is not commonly utilized in industrial applications due to its low strength [13]. Mg_2Si is an intermetallic compound with the potential to enhance the properties of Al alloys. This is because it possesses a high hardness (in the range of $4.5 \times 10^9 \text{ Nm}^{-2}$) and elastic modulus (120 GPa), as well as low density (1.9 g/cc), and high melting temperature ($1085 \text{ }^\circ\text{C}$) [14]. Mg_2Si also has a better oxidation resistance compared to magnesium alloys due to its high silicon content [15]. By providing a perfect combination of physical and mechanical properties when used as reinforcement in $\text{Mg}_2\text{Si}/\text{Al}$ and $\text{Mg}_2\text{Si}/\text{Mg}$ composites, it can allow for the production of promising candidate materials used for automobile, aerospace, biomedicine, and other applications [16]. However, this intermetallic compound is highly brittle, especially at low temperatures. Other researchers stated that a plausible reason for this brittleness is the coarse dendritic structure formed in the Mg_2Si phase during the solidification process of Al or Mg melts [17]. The brittleness of the Mg_2Si phase increased the tendency of this intermetallic compound to act as a stress-concentration region, which induces the nucleation and propagation of cracks and deteriorates the respective properties, such as machinability, mechanical properties and wear resistance [18]. This has led to many studies being conducted to modify the Mg_2Si phase so that the strength and ductility of the alloy can be enhanced.

On the other hand, some research had also been carried out to examine the influence that the addition of ceramic particles has on the alterations in the size and morphology of Mg_2Si particles in Al- Mg_2Si composites using an ex situ technique. According to [19], nano-sized SiC particulates and in situ Mg_2Si particles reinforcing the Al-Cu matrix were used to fabricate the hybrid composites, and the microstructure and mechanical properties were investigated. In this study, a comparison was made between the properties Al-Cu alloy, $\text{Mg}_2\text{Si}/\text{Al-Cu}$, SiC/Al-Cu, and $(\text{Mg}_2\text{Si} + \text{SiC})/\text{Al-Cu}$ composites. The researchers showed that the mixing of in situ Mg_2Si and ex situ SiC can effectively alter the morphology of the Mg_2Si particles by changing them from a short strip to a dot shape. The results indicate that, after the addition of SiC, the primary α -Al phase in the $(\text{Mg}_2\text{Si} + \text{SiC})/\text{Al-Cu}$ hybrid composite was significantly refined as compared to that of the $\text{Mg}_2\text{Si}/\text{Al-Cu}$ composite. It was also found that the grain size of the $\text{Mg}_2\text{Si}/\text{Al-Cu}$ and $(\text{Mg}_2\text{Si} + \text{SiC})/\text{Al-Cu}$ composites was greatly reduced relative to that of the Al-Cu alloy. This indicates that SiC and Mg_2Si phases can deter the growth of primary Al grains. In addition, the size of the Mg_2Si particles is also refined by the addition of SiC. This can be explained by the phenomenon whereby SiC can act as the nucleus of Mg_2Si to allow for heterogeneous nucleation to take place during solidification. In addition, SiC particles acted as a physical barrier in the growth stage of Mg_2Si particles; therefore, the grain size of Mg_2Si was reduced [20]. Furthermore, the addition of SiC to the $\text{Mg}_2\text{Si}/\text{Al-Cu}$ composite also decreases the ductility of the composite, since SiC particles are considered to be hard and brittle [19]. Another study was focused on comparing the characteristics of ADC-12 (AA383) reinforced with nano-SiC and nano- Al_2O_3

composites fabricated by the stir-casting method. The variations in the amount of nano-SiC and nano- Al_2O_3 that was added were 0.05, 0.1, 0.15, 0.2, and 0.3 vf. %. It was found that nano-SiC and nano- Al_2O_3 reduced the primary Al grain size as they act as a grain-refiner. Furthermore, the addition of nano-SiC and nano- Al_2O_3 improved the hardness value while decreasing the wear rate. This can be explained by the higher hardness of the particles compared to the matrix, which hardens the composites [21]. Moktar et al. [20] found that when Al-20%Mg₂Si composite is added with 10 wt.% SiC, the primary Mg₂Si morphology changed to polygonal, together with a decrease in its size to 30 μm . The ability of the stir-casting method to produce Al6061-SiC- Al_2O_3 hybrid composites was reported by Umanath et al. [22]. They found that, with the addition of reinforcement particles to the alloy matrix, microhardness increases due to the solid solution hardening of the matrix. The microstructure and tensile properties of Al_2O_3 /SiCp-reinforced AMMCs produced by stir-casting were evaluated by Altinkok et al. [23]. Compared to the unreinforced alloy, the strength of the hybrid composite was higher; the considerable improvement in the tensile strength of the composites was associated with the reinforcement shape, grain and particle size, as well as the uniform distribution of the particles in the matrix. Uvaraja et al. [24] concentrated on the wear behavior of hybrid composites by altering the SiC contents and fix content of B_4C particles. The increase in the hardness of the composite was believed to mainly be due to the presence of hard B_4C and SiC in the alloy matrix, which act as a barrier to the dislocation movement. An examination of the metallography and bulk hardness of artificially aged Al6061- B_4C -SiC hybrid composites was conducted by Sharma et al. [25]. Compared to the aluminum alloy, a considerable enhancement in tensile strength and hardness, and a minimal decrease in the ductility of hybrid composites were detected. Uthayakumar et al. [26] examined the dry sliding wear performance of Al1100-SiC- B_4C hybrid composites. Due to the existence of hard B_4C and SiC particles in the matrix alloy, an increase in hardness and wear resistance was observed. The literature review indicated little research studying the effect of YSZ particles on the microstructure and characteristics of Al-Mg₂Si composite, such as wear behavior, hardness level, and corrosion resistance. This is because most articles focused on the Al matrix reinforced with materials such as SiC, Al_2O_3 , B_4C , etc. To cover this gap in the science, the primary focus of this research is to examine the microstructural alterations in Al-15%Mg₂Si composites with various YSZ contents. In addition, the hardness and sliding wear behavior of Al-15%Mg₂Si composites following YSZ additions is investigated. The secondary goal is to evaluate the corrosion properties of Al-15%Mg₂Si-xYSZ hybrid composites.

2. Materials and Methods

2.1. Fabrication Process of Materials

The base material, Al-15%Mg₂Si, was prepared in advance with pure Al (99.9%), pure Mg (99.9%), and pure Si (98.9%). A resistance furnace was used to melt the pure Al and Si in a crucible at 800 °C. The pure Mg was added to the melt material contents at the temperature drop of 750 °C. After dissolution and homogenization, the molten material was poured into the steel mold and completely solidified to form the Al-15%Mg₂Si ingot. Afterward, the ingot was cut into smaller sections for the subsequent stir-casting procedure. The YSZ powder was preheated using a muffle furnace at 800 °C for 2 h to enhance the wettability. The mass fractions of the YSZ powder were then accordingly divided into 0, 3, 6, and 9 wt.%. Then, a resistance furnace was used to melt the Al-15% Mg₂Si ingot in a crucible at the temperature of 750 °C. YSZ powders of 3, 6, and 9 wt.% were gradually added to the melt at 750 °C with a uniform stirring action to ensure the even dispersion of YSZ particles in the melts. The melts were then held for 15 min before being reheated to 720 °C and subsequently cast in the steel die to produce samples for further characterization and testing.

2.2. Microstructural Characterization

Microstructure characterization was performed on the composite materials fabricated using an optical microscope (OM) and scanning electron microscope (SEM) equipped with energy-dispersive X-ray spectroscopy analysis (EDS). Through optical microscopy, observations were made to identify the microstructural alterations in the fabricated materials. This procedure was followed by quantitative analysis (using an i-Solution image analyzer), where measurements of the size and aspect ratios of primary Mg₂Si particles were carried out. These values of individual particle sizes were recorded using Equations (1) and (2), and the average values were taken.

$$\text{Mean particle size} = \frac{1}{m} \sum_{j=1}^m \left(\frac{1}{n} \sum_{i=1}^n L_i \right)_i \quad (1)$$

$$\text{Aspect ratio} = \frac{1}{m} \sum_{j=1}^m \left(\frac{1}{n} \sum_{i=1}^n \frac{a_i}{b_i} \right)_i \quad (2)$$

where the parameter size is L_i , and parameters a_i and b_i are the longest and shortest dimensions of a single Mg₂Si particle, respectively; n is the number of Mg₂Si particles measured in a single field (0.60126 mm²), while m is the number of the evaluated field.

SEM was employed to investigate the microstructure with a greater resolution and larger field depth, as well as the worn surfaces of the fabricated composites. In addition, EDS analysis was used to identify the elements present in the composite materials.

2.3. Hardness Test

The hardness test was carried out using a Vickers hardness tester. After specifying the loads applied by the indenter onto the samples, which were 5 kg with a continuous dwelling for approximately 30 s, the hardness values were obtained, followed by the measurement of the depth of indentation into the samples applied by the tester. Several points (a minimum of 10 points spread across the surface) were chosen to be indented, and the average value was calculated for further analysis.

2.4. Sliding Wear Test

A wear test was carried out to study the alterations in the dimensions experienced by the material after being exposed to continuous sliding or rolling action for a certain amount of time. Linear Reciprocating Tribometer (manufactured by DUCOM Instruments PVT. LTD) was employed. A floor-standing model with the capacity to determine the frictional force and coefficient of friction, which can then be used to identify the wear characteristics of the samples, was utilized. The machine works by pressing the top specimen (test samples) on the bottom specimen (made of mild steel) under dry conditions, in which the top specimen is in a constant linear reciprocating motion while in contact with the bottom specimen. The parameters were set before conducting the test, which encompasses the normal applied load (25 and 50 N), frequency (2 Hz), stroke length (10 mm), and test duration (30 min). In this study, the applied load was set as the manipulating variable, while the frequency, stroke length, and test duration were fixed to identify the wear properties of the materials. The samples used in this test were 15 mm long cylindrical pin form, with a 6 mm diameter, whereas the bottom specimen was a square plate of 40 mm side length, fabricated according to the ASTM G-133 standard. The pin samples were weighed before and after the test to identify the weight loss caused by the wear process. In addition, the surfaces of the pins and plate in contact were cleaned with acetone both before and after the wear test. After fixing the pin and plate in their respective holders, the pin was then placed onto the plate and underwent a linear reciprocating motion for a pre-determined time to induce wear on the pin surface. Through the Winducom 2010 software, the values of frictional force and coefficient of friction were recorded with as many as 10 data points

saved per second. By using the weight loss value, which is the weight difference before and after the wear test, the volume loss can be calculated using the following expression:

$$\text{Volume loss (mm}^3\text{)} = \frac{\text{Weight loss (g)}}{\text{Density (}\frac{\text{g}}{\text{cm}^3}\text{)}} \times 100 \quad (3)$$

The volumetric wear rate can then be computed using the following equation.

$$\text{Volumetric wear rate (mm}^3\text{/km)} = \frac{\text{Volume loss (mm}^3\text{)}}{\text{Sliding distance (km)}} \quad (4)$$

Equations (3) and (4) were utilized to compute the wear rates of different materials of interest in this study [27].

After the wear test, the pin samples were cleaned in an ultrasonic cleaning machine to remove unwanted wear debris from the worn surfaces. The worn surfaces were then analyzed using variable pressure scanning electron microscopy (VPSEM) to identify the corresponding wear mechanisms.

2.5. Corrosion Test

An electrochemical test was carried out to determine the corrosion behavior of the composite materials. The test was implemented using a three-electrode cell consisting of a reference electrode (Ag, AgCl/KCl (3.5 M)), a counter-electrode (made of a graphite rod), and a working electrode (the specimen with a surface area of 1 cm²). These electrodes were immersed in a 60 mL 3.5% NaCl solution, at 25 °C and in the open air, along with the set-up of a VersaSTAT 3F potentiostat/galvanostat. The results were then analyzed and displayed using VersaStudio software. The tests were accomplished with a scan rate of 0.2 mV/s (constant) and within a fixed range of potential: −250 mV to +250 mV in reference to the open circuit potential.

3. Results and Discussion

3.1. Microstructural Characterization

The microstructures of the Al-15%Mg₂Si composites with different YSZ reinforcement concentrations (0, 3, 6, and 9 wt.%) are shown in Figure 1. The blue phases in the images are the primary Mg₂Si particles, while the dark phases in Figure 1b–d are YSZ particles. It can be observed that as the YSZ content increases, the quantity of dark phases also increases, with an even, satisfactory distribution throughout the matrix. Furthermore, it can also be observed that the mean size of the primary Mg₂Si particles exhibits a decremental trend as the YSZ addition increases from 0 to 9 wt.% (Figure 1a–d).

In terms of the morphology of the primary Mg₂Si material particles, the particles had a dendritic shape for the as-cast Al-15%Mg₂Si composite (Figure 1a). In the Al-15%Mg₂Si-3 wt.% YSZ hybrid composite, a slight variation in the morphology could be seen, ranging from a dendritic to polygonal shape, as observed in Figure 1b. Most of the primary Mg₂Si particles transformed to a polygonal shape following the addition of 6 and 9 wt.% YSZ to the composite (Figure 1c,d). This morphological change occurs as the presence of YSZ alters the growth mode of Mg₂Si during the solidification process. A similar observation was reported following the addition of chromium (Cr), which affects the morphology of the Mg₂Si content in the Al-15%Mg₂Si material [28].

The increase in YSZ particles boosts the number of heterogeneous nucleation zones in the primary Mg₂Si phase. As more nucleation sites are present, more of the primary Mg₂Si phase forms, which leads to a higher density, and smaller and more uniform distribution of the primary Mg₂Si phase [29]. Another reason for the refinement of primary Mg₂Si particles in YSZ particles is the role that YSZ particles play as a physical barrier during the growth of the primary Mg₂Si phase through solidification. Based on the particle-pushing phenomenon, a solidification front rejects the B₄C particles, and they finally

become stuck in the grain boundary areas [24,26]. The corresponding elemental mapping of Al-15%Mg₂Si-9 wt.% YSZ and related EDS analysis are illustrated in Figure 2 and Table 1, respectively. These show that the microstructures consist of α -Al as the matrix and Mg₂Si and YSZ phases as the reinforcements. Moreover, the YSZ particles are evenly distributed throughout the matrix. In addition, the primary Mg₂Si phase, based on the equilibrium phase diagram, is the primary phase formed during the process of solidification, which is then followed by the co-solidification of α -Al and eutectic Mg₂Si phases from the liquid alloy, as indicated in the narrow, ternary-phase region [30]. To allow this co-solidification to take place, the primary Mg₂Si particles act as the heterogeneous nucleation sites for α -Al. After this, a pseudo-eutectic phase consisting of Al and Mg₂Si will form around the α -Al [31]. This can be observed in Figure 2, where the primary Mg₂Si particles are surrounded by α -Al, which is then covered by another phase composed of eutectic Al and Mg₂Si.

Furthermore, the SEM images for the Al-15%Mg₂Si in situ composite reinforced with 0, 3, 6, and 9 wt.% YSZ are depicted in Figure 3 for comparison purposes. As can be observed in Figure 3a, the primary Mg₂Si particles have large and irregular dendritic structures, which are surrounded by α -Al and eutectic Mg₂Si. The addition of 3 wt.% YSZ causes the primary Mg₂Si particles to become smaller in size, but their dendritic morphology is still present, as illustrated in Figure 3b. With the addition of 6 and 9 wt.% YSZ, the particles are greatly refined, as shown in Figure 3c,d, which correlates well with the reduction in average size and aspect ratio, as presented in the previous section. The YSZ phase is concentrated in the interface between the Mg₂Si crystals and the Al matrix, which reduces the surface energy of the Mg₂Si growth front and increases the local super-cooling composition. When the content of YSZ is adequately high, a rapid cooling of the melt during the solidification process results in an insufficient time for the diffusion of YSZ into the liquid phase. This ultimately forms a YSZ-rich layer that slows down the growth of Mg₂Si [32,33]. Hence, this proves that the addition of YSZ has a positive effect on the microstructures of the materials through refinement and the uniform dispersion of the primary Mg₂Si particles in the hybrid composites.

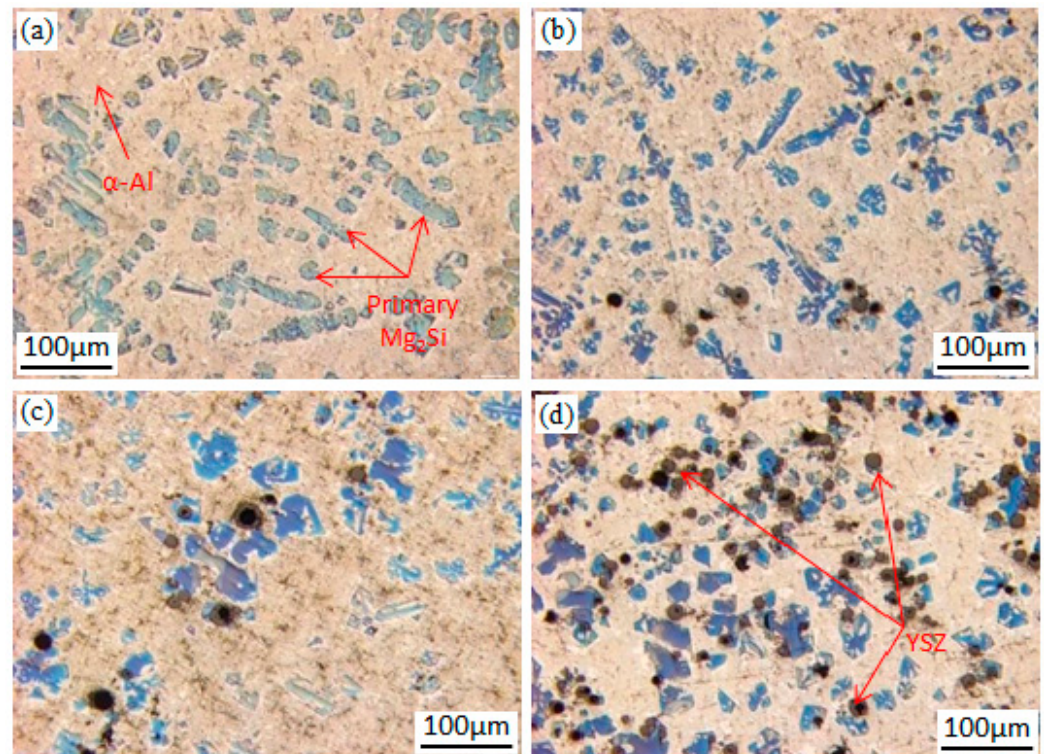
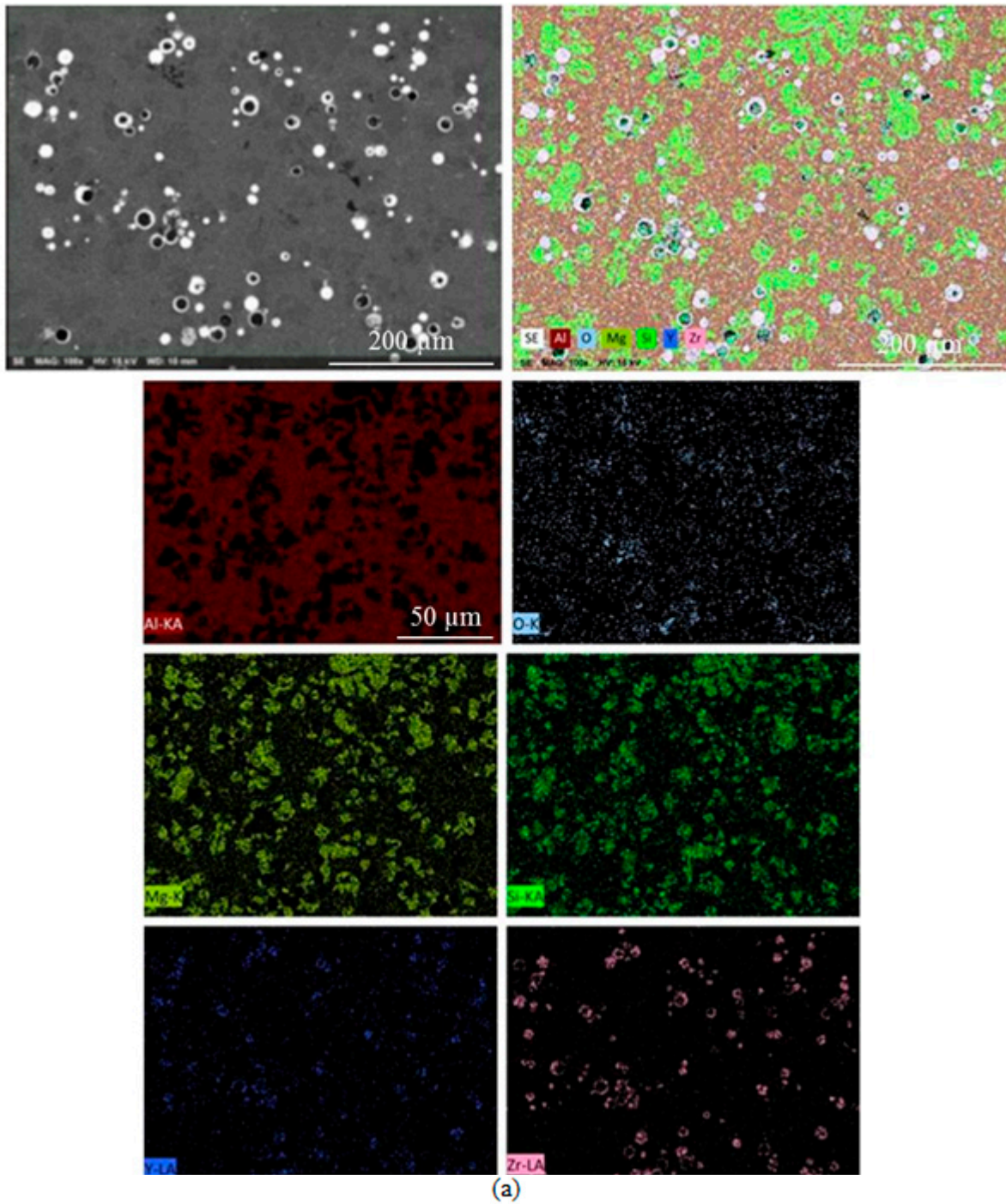


Figure 1. Optical micrographs of Al-15%Mg₂Si composite material with various YSZ contents: (a) 0, (b) 3, (c) 6, and (d) 9 wt.%.



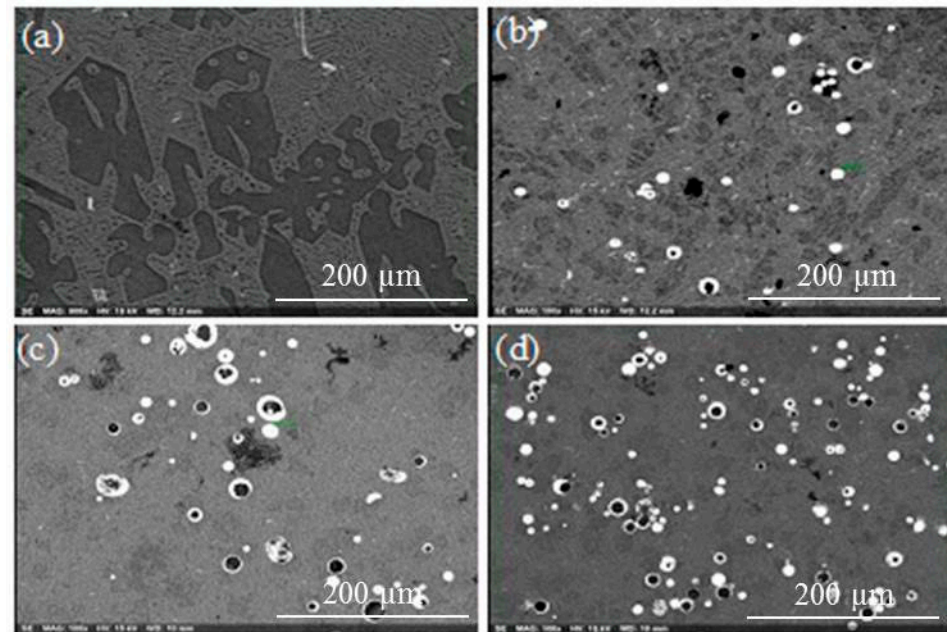
Element	At. No.	Line s.	Netto	Mass [%]	Mass Norm. [%]	Atom [%]	abs. error [%] (1 sigma)	abs. error [%] (2 sigma)	abs. error [%] (3 sigma)
Zirconium	40	L-Series	40610	11.14	67.81	31.04	0.45	0.89	1.34
Oxygen	8	K-Series	4291	4.08	24.83	64.80	0.68	1.36	2.04
Yttrium	39	L-Series	4124	1.12	6.81	3.20	0.07	0.15	0.22
Magnesium	12	K-Series	116	0.09	0.56	0.96	0.04	0.07	0.11
			Sum	16.42	100.00	100.00			

(b)

Figure 2. (a) Elemental mapping analysis of Al-15%Mg₂Si-9 wt.% YSZ hybrid composite and (b) corresponding EDS analysis of YSZ particles.

Table 1. EDS analysis of YSZ particles.

	Mass (%)	Mass Norm. (%)	Atom (%)	Abs. Error [%] (1 Sigma)
Zirconium	11.14	67.81	31.04	0.45
Oxygen	4.08	24.83	64.80	0.68
Yttrium	1.12	6.81	3.20	0.07
Magnesium	0.09	0.56	0.96	0.04

**Figure 3.** SEM micrographs of Al-15%Mg₂Si reinforced with: (a) 0, (b) 3, (c) 6, and (d) 9 wt.% YSZ.

3.2. Quantitative Analysis of the Microstructure

By analyzing the optical micrographs using the image analyzer, the average sizes and aspect ratios of the primary Mg₂Si particles in the in situ composites with different YSZ reinforcements were measured, as shown in Figure 4. The average sizes of the primary Mg₂Si particles with the addition of 0, 3, 6, and 9 wt.% YSZ are 137.78 μm, 123.04 μm, 103.06 μm, and 88.36 μm, respectively. The average size shows a decremental trend as more YSZ is added. These results are in accordance with the observations made by the optical micrographs (Figure 1). The reduction in size may be due to YSZ particles' suppression of the anisotropic growth of the primary Mg₂Si phases, either through poisoning the Mg₂Si nuclei by distributing the YSZ particles at the liquid–solid interface or by distorting the lattice structure of Mg₂Si by altering the Mg₂Si crystals' surface energy [31]. The average aspect ratio of the primary Mg₂Si particles was also calculated. The results are as follows: 3.00 (0 wt.% YSZ), 2.75 (3 wt.% YSZ), 1.81 (6 wt.% YSZ), and 1.27 (9 wt.% YSZ). The aspect ratios decreased as the content of YSZ increased up to 9 wt.%. The lower aspect ratio can be attributed to the restricted growth theory, which states that the YSZ particles can restrict and regulate the growth of primary Mg₂Si according to their dispersion at the solid–liquid interface [34]. Two different mechanisms contribute to the modification of the primary Mg₂Si particles, namely, heterogeneous nucleation and the poisoning effect.

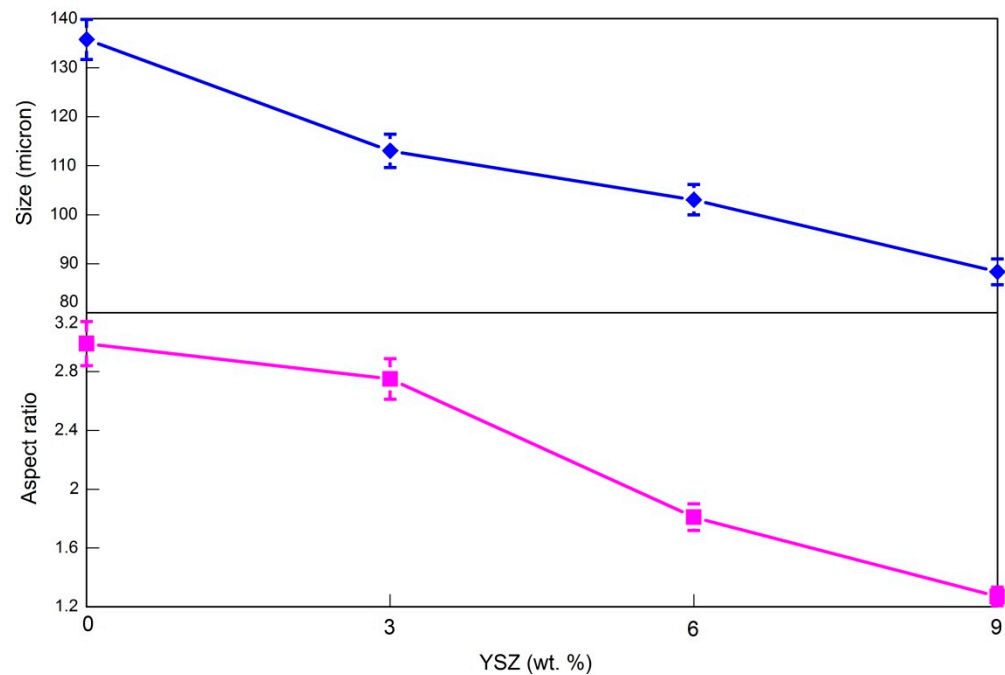


Figure 4. Average size and aspect ratio of primary Mg_2Si particles in Al-15% Mg_2Si composite with different amounts of YSZ.

In the first case, the modifier elements (or the containing compounds) serve as the heterogeneous nucleation sites, while in the second case, the modifier elements are absorbed by the growth front of the primary phase, hence restricting its preferred growth direction [35]. By identifying the compounds formed between YSZ and the melt during the initial stage of the solidification process, the lattice misfit between the mentioned compounds and the primary Mg_2Si phase can be calculated using Bragg's theory. If the computed misfit value is below 15%, then one phase is capable of acting as the heterogeneous nucleation site for the other phase [36].

Another mechanism is the poisoning effect caused by the modifier elements or the compounds. This may occur as the modifying particles can adsorb to the growth planes of the primary Mg_2Si phase to subsequently distort the Mg_2Si lattice [37] and alter the surface energy of the phase [38]. However, determining the new phase formed in the interface of Al-YSZ and calculating the misfit value, as well as its poisoning effect, requires further investigation.

3.3. Hardness Test

The mean Vickers hardness values of the materials were measured and computed. With the increase in YSZ content in the composites, the average hardness values displayed an incremental trend, increasing from 102.72 HV in the as-cast Al-15% Mg_2Si composite to 125.63 HV with the addition of 3% YSZ, and continuing to elevate to 125.73 HV and 126.44 HV for 6% and 9% YSZ contents, respectively, as depicted in Figure 5. As shown in the preceding results, the average sizes and aspect ratios of the primary Mg_2Si phase reduced as more YSZ was added to the as-cast composite. This explains the phenomenon of hardness values increasing with an increase in YSZ content. The YSZ particles, besides providing Mg_2Si phase refinement in the hybrid composites, also help to boost the hardness by impeding the sliding motion of the grain boundary. Another contributing factor is the resulting mismatch in thermal expansion between the matrix and the reinforcement at the interfaces, which potentially intensifies the dislocation pattern in the material [32]. According to other researchers, other possible contributing factors include the finer hard primary phases in the matrix, as well as the increase in obstacles to the grain boundary sliding, and the higher quantity of Mg_2Si being exposed to the indenter [35].

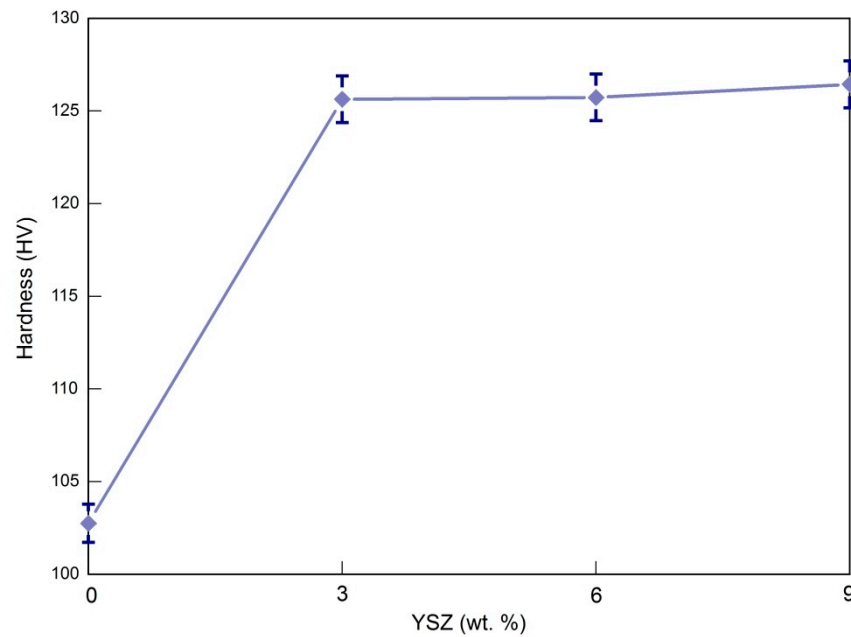


Figure 5. The Vickers hardness of the Al-15%Mg₂Si composite treated with different YSZ particle contents.

3.4. Wear Test

The volumetric wear rate of the studied materials is displayed in Figure 6. It can be observed that as the content of YSZ increased from 0% to 9 wt.%, the wear rate tended to reduce, and a similar trend is exhibited for both 25 N and 50 N applied loads. This enhancement is the outcome of the load capacity of the composites caused by the ceramic particles during sliding. Under the 25 N applied load, the lowest wear rate was attained at 9 wt.% of YSZ with a value of 0.46 mm³/km, while for the 50 N load, the minimum wear rate was also achieved at 9 wt.% of YSZ with a value of 1.22 mm³/km. This reduction in wear rate, or, in other words, improvement in wear resistance, can be explained by the hardness of the materials. This can be further verified by matching the wear rate with the average hardness values. Since Al-15%Mg₂Si-9%YSZ has the highest hardness value, it is expected to possess the best wear resistance in comparison with other materials with lower YSZ contents. The calculated wear rate proves that this is the case. The relationship between wear rate and hardness can be demonstrated by Archard’s law, which is as follows:

$$Q = \frac{KW}{H} \tag{5}$$

In Equation (5) Q is the wear rate in mm³/km, parameter K is the wear coefficient, variable W is the volume of worn material per distance, and parameter H is the hardness according to the Vickers scale. According to this relation, it can be concluded that the wear rate is directly related to the hardness of the materials [39]. Another reason for the reduction in the wear rate of the composite is the refinement of the primary Mg₂Si particles, as illustrated in Figures 1 and 4. It was anticipated that, during the wear test, the hybrid composite with finer Mg₂Si particles would have a lower wear rate due to the grain boundary strengthening that occurs with a smaller particle size, which results in strain-hardening [40]. Figure 6 also shows that the wear rate is increased when the applied load increases from 25 N to 50 N. In fact, at higher loads, the number of contact asperities and the separation of surface asperities increases. Furthermore, with an increase in the applied load, wear debris accumulate in the space between the disc and pin, resulting in more serious abrasive wear, increasing the wear rate.

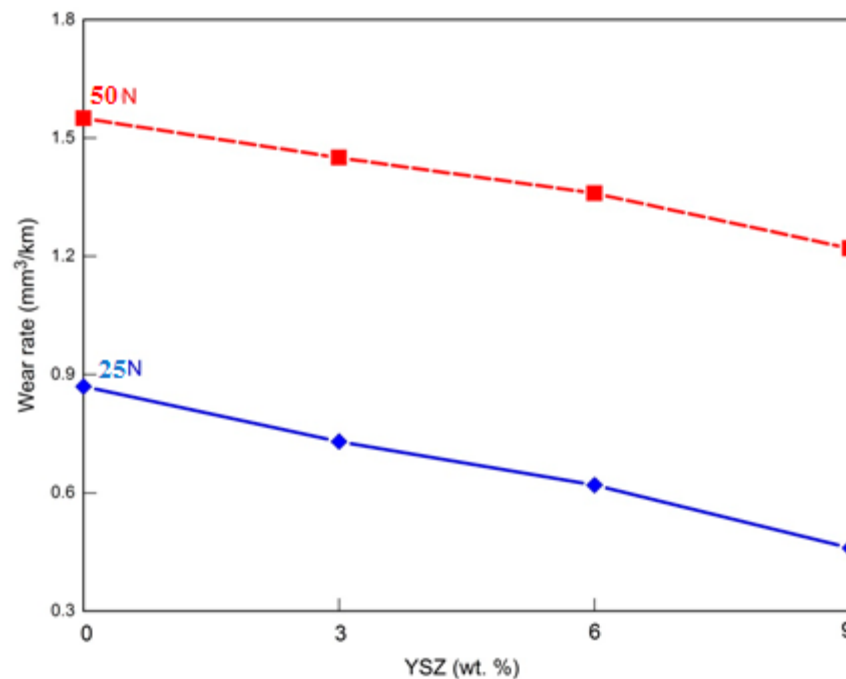


Figure 6. Volumetric wear rate versus the YSZ contents under 25 N and 50 N applied loads.

Figure 7 demonstrates the average coefficient of friction (COF) values of fabricated composites. A descending trend can be observed with the addition of YSZ particles from 0 wt.% to 9 wt.%. This particular trend could be related to the improved hardness value when more YSZ is present in the composite materials, as well as the finer primary Mg_2Si particles. This may be the case, as harder materials can withstand a higher load and prevent the expansion that occurs when the surface between the pin and the plate is contacted. This indirectly prevents the pin surface from obtaining more scratches. As a result, fewer scratches and wear deformations will form on the pin surface during the wear process [41]. Hence, the Al-15% Mg_2Si -9%YSZ hybrid composite has the lowest COF in comparison to other composite materials. The high COF of the as-cast Al-15% Mg_2Si composite YSZ can be ascribed to the damage caused to both the primary and eutectic Mg_2Si particles, as well as finer particles, throughout the wear process. In addition, the Mg_2Si particles are unable to withstand the deformation caused by the wearing process. Therefore, cracks can propagate with greater ease in the matrix, resulting in the pullout of the Mg_2Si particles. These particles later act as hard abrasives that further elevate the COF [27]. With an increase in the load applied to 50 N, the COF increases compared to the load applied to 25 N. Nevertheless, the Al-15% Mg_2Si -9% YSZ hybrid composite has the lowest COF (0.50) in comparison with other fabricated composites, similar to the COF trend of composites under 25 N.

Figure 8(a1) illustrates the worn surface of the as-cast Al-15% Mg_2Si composite under 25 N applied load. From the worn surface, the main wear mechanisms were shown to include abrasion and delamination. This is exemplified by the presence of deep and wide ploughing grooves along the wear-sliding direction. These wide grooves are characteristic of the severe abrasion caused by the hard asperities on the steel plate or pulled-out hard particles that act as wear debris. Once the counterfaces between the sample surface and pin increase, more materials detach from the surface of the samples. This detachment could be related to the adhesive friction that consequently increases the wear rate (Figure 6). The observation could also suggest a mixed mode of two-body and three-body abrasions that produce wide grooves [26]. These grooves are formed after pulling out of the fractured primary Mg_2Si dendrites. Delamination is caused by the fractured eutectic Mg_2Si as a result of the unbearable stress exerted on the surface between the pin and plate. With the increase in the load to 50 N, the wear mechanisms shift to adhesion and delamination wear mechanisms (in which extensive pits and large delamination flakes exist on the worn

surface), leading to a higher amount of material removal (Figure 8(b1)), in accordance with the wear rate shown in Figure 6 and the higher weight loss found after the wear test. The higher load also forces an enormous amount of abrasives to become entrapped in the cavities, which promotes more intensive scratching actions on the surface during wear [41]. This high amount of material removal may be related to the material's low shear strength and fracture toughness without the use of YSZ particles as a reinforcement [27].

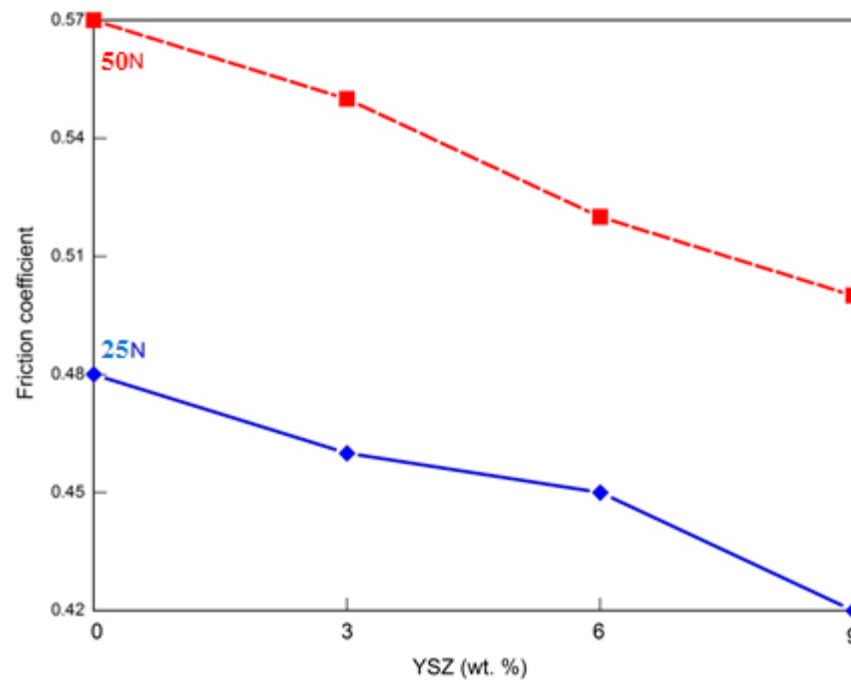


Figure 7. Coefficient of friction (COF) of the fabricated composites with a test duration of 0, 3%, 6%, and 9 wt.% YSZ.

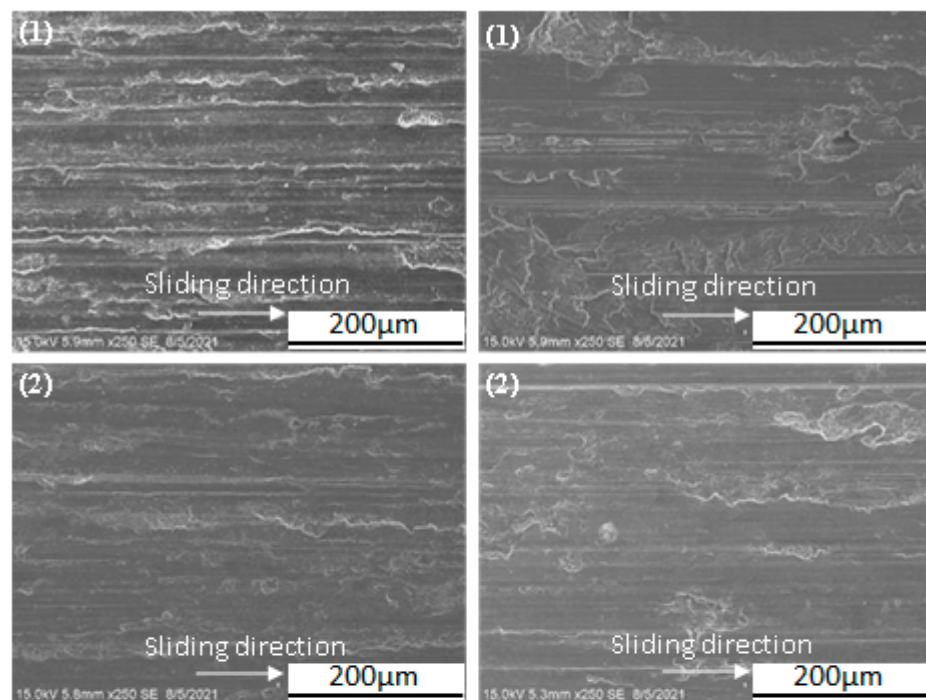


Figure 8. Cont.

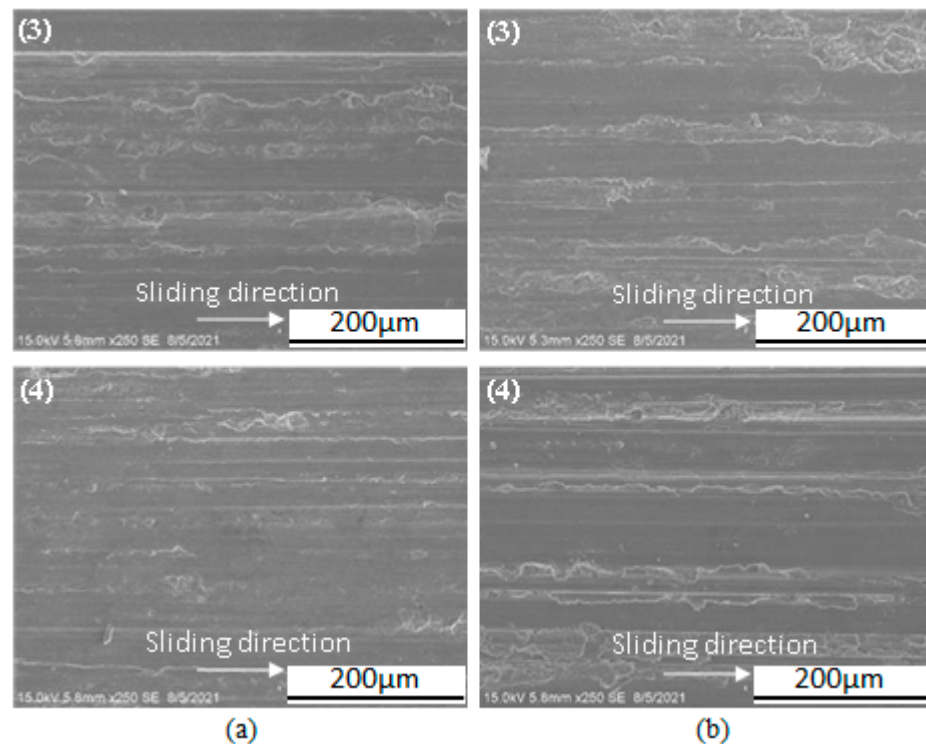


Figure 8. SEM images of the worn surfaces of Al-15%Mg₂Si composite under (a) 25 N and (b) 50 N of applied load with different YSZ contents: (1) 0, (2) 3 wt.%, (3) 6 wt.%, and (4) 9 wt.%.

When YSZ is incorporated into the as-cast Al-15%Mg₂Si composite, the worn surface is observed to be smoother with noticeably narrower grooves and shallower pits (Figure 8(a2–b4)). This is expected because the wear rate shows a decreasing trend as more YSZ reinforcement is incorporated into the as-cast composite, as illustrated in Figure 6. Nevertheless, delamination still occurs, as can be seen in Figure 8(a2–a4,b2–b4), but this phenomenon becomes milder as more YSZ is added. Figure 8(a4,b4) depicts the worn surface of Al-15%Mg₂Si -9%YSZ under 25 N and 50 N applied loads, respectively. Compared to the preceding samples, grooves with a smaller depth and width, in addition to the absence of delamination (illustrating a mild abrasive wear mechanism), indicate that the material possesses a better wear resistance. This enhanced property can be credited to the improved hardness caused by the contribution of the refined Mg₂Si particles and their more even distribution within the matrix. In addition, the refinement of the Mg₂Si particles also permits the formation of a rough reinforcement–matrix interface, which obstructs the initiation and propagation of cracks [18,42].

3.5. Corrosion Test

An electrochemical (polarization) test was carried out to investigate the corrosion behavior of the Al-15%Mg₂Si with various YSZ concentrations; the results are presented in Figure 9. This clearly demonstrates that the addition of YSZ can alter the corrosion resistance of the composite. The electrochemical kinetic parameters, including the corrosion potential (E_{corr}) and the corrosion current density (i_{corr}), are tabulated in Table 2. The corrosion current density of the as-cast Al-15%Mg₂Si composite is recorded at $5.62 \mu\text{A}/\text{cm}^2$, which is a high value. On the other hand, when 9 wt.% of YSZ is added, the corrosion current density value drops notably to $2.74 \mu\text{A}/\text{cm}^2$. This confirms that the addition of YSZ as the reinforcing phase improves the corrosion resistance of Al-15%Mg₂Si.

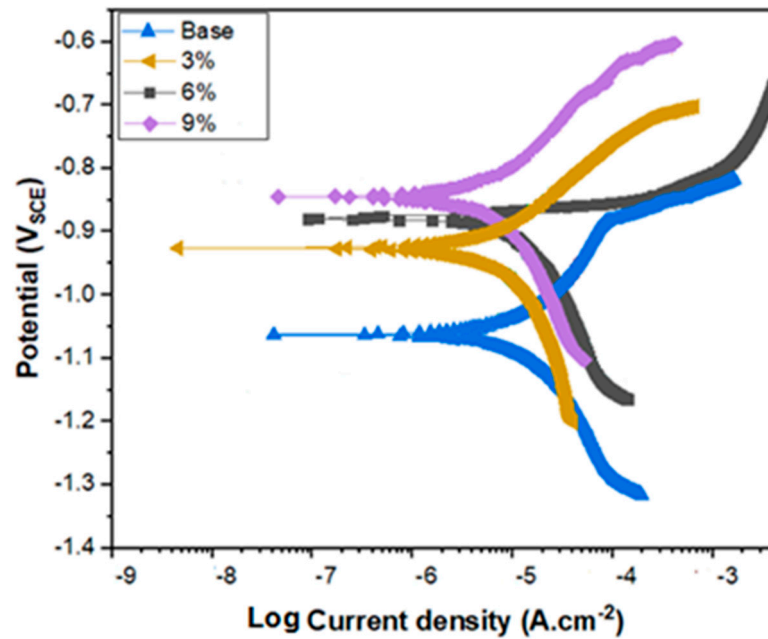


Figure 9. Polarization curve of Al-Mg₂Si-xYSZ in 3.5% NaCl solution.

Table 2. Electrochemical kinetic parameters of Al-15%Mg₂Si-xYSZ hybrid composites.

Content of YSZ (wt.%)	E _{corr} (mV)	I _{corr} (μA/cm ²)	Corrosion Rates (mmpy)
0	−1061.20	5.62	0.164
3	−908.98	3.02	0.089
6	−913.64	7.46	0.217
9	−839.96	2.74	0.080

Furthermore, the relationship between the corrosion rate and YSZ content is demonstrated in Figure 10. These values indicate the same finding, which further validates that the addition of YSZ can reduce the corrosion rate, or, in other words, boost the corrosion resistance of the material. The corrosion properties of Al alloys/composites mainly depend on the size, number and chemical composition of the precipitates [43]. The corrosion potential of Mg₂Si is negative, showing that Mg₂Si particles are more susceptible to corrosion [44]. With the addition of 9 wt.% YSZ to the Al-15%Mg₂Si composite, the average size of primary Mg₂Si particles showed a larger decrease compared to other fabricated composites, which reduces the susceptibility of these particles to corrosion. Hence, improvements in the corrosion behavior of the Al-15%Mg₂Si composite with the addition of YSZ can be linked to the more refined and evenly distributed Mg₂Si particles found in the composite, which inhibit the propagation of corrosion pits (Farahany et al., 2020) [41]. These corrosion pits propagate through the inner channels into the matrix. The presence of fine and uniformly dispersed reinforcement particles can obstruct the channels, which increases the pits' difficulty propagating [45].

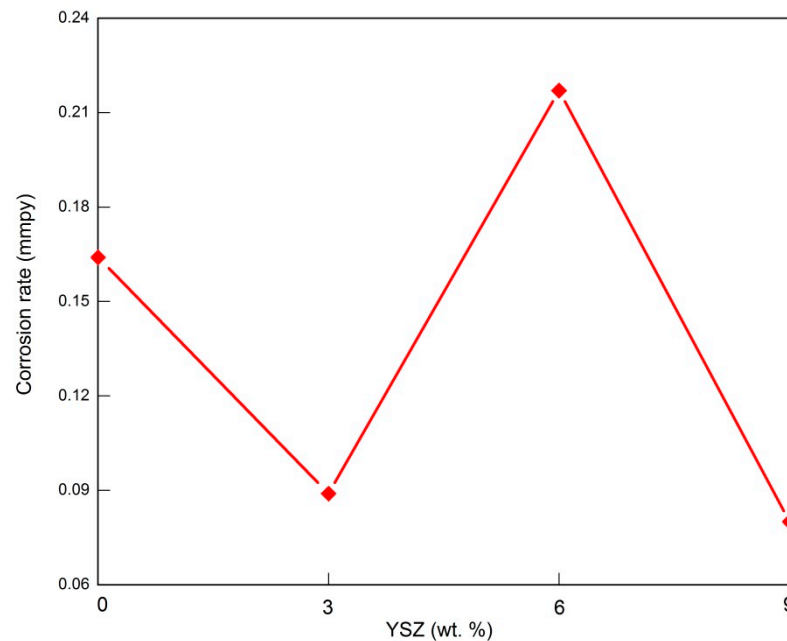


Figure 10. Corrosion rate of the Al-15%Mg₂Si composite with various quantities of YSZ.

4. Conclusions

The literature review highlights a limited study on the effect that YSZ particles have on the properties of the Al-Mg₂Si composite. In this study, the Al-15%Mg₂Si hybrid composite materials with various quantities of YSZ particles were produced using in situ and ex situ techniques. Then, the microstructural features, hardness, wear, and corrosion properties of the fabricated composites were examined. The main findings are concluded as follows:

- Microstructural examination revealed that the addition of YSZ particles successfully refines the size of primary Mg₂Si phases, as well as providing an even distribution of these phases across the Al matrix. Among the fabricated composites, the Al-15%Mg₂Si-9%YSZ hybrid composite demonstrated the best outcome, with the most apparent effect in terms of particle refinement and phase distribution. The size reduction is as much as 35.87%, while the aspect ratio decreased by 57.67% compared with the as-cast, in situ composite.
- Furthermore, the hardest composite was found to be Al-15%Mg₂Si with 9% of YSZ, for which a hardness value of 126.44 HV was recorded, compared to the as-cast composite, with a hardness value of 102.72 HV. This hardness level can be attributed to the finer primary Mg₂Si phases and hard YSZ-reinforcing particles that pin the sliding of grain boundaries.
- Both results regarding the wear rate, as well as the coefficient of friction, imply that the in situ Al-15%Mg₂Si composite with 9wt.% YSZ content demonstrates the best wear resistance. In addition, the SEM images of the worn surfaces also reveal that the Al-15%Mg₂Si-9%YSZ hybrid composite showcases the least severe wear, with only mild abrasions on the smoothest surface. This excellent wear behavior may be credited to the high hardness, along with the refined and uniform distribution, of the Mg₂Si particles in the composite.
- The electrochemical test result suggests that the Al-15%Mg₂Si-9%YSZ hybrid composite possesses better corrosion resistance than the as-cast composite and composites with 3, 6wt.% YSZ. This is as expected since the optimum size and dispersion of Mg₂Si particles can impede the propagation of corrosion pits initiated on the surface of the material.
- Further investigations of the thermal behavior and other mechanical properties of hypereutectic Al-Mg₂Si composites are recommended for further studies.

Author Contributions: Conceptualization, investigation, data curation, and writing—original draft were performed by H.G.; validation, visualization, methodology, formal analysis, and revision/review/editing—original draft were performed by H.G., M.A.J., M.P., T.A.A.B., L.J.L. and S.S.R.K.; supervision, project administrations, resources, and funding acquisition was performed by H.G., M.P., T.A.A.B. and S.S.R.K. All authors have read and agreed to the published version of the manuscript.

Funding: This research received no external funding.

Institutional Review Board Statement: Not applicable.

Informed Consent Statement: Not applicable.

Data Availability Statement: Not applicable.

Acknowledgments: The authors would like to express their appreciation to New Uzbekistan University (NUU), Universiti Teknologi Malaysia (UTM) for providing research facilities and the Ministry of Higher Education for their financial support under the Fundamental Research Grant Scheme (FRGS) Registration Proposal No: FRGS/1/2022/TK10/UTM/02/45. The author acknowledges the support of the Minister of Transport and Construction of the Slovak Republic and the European Union in the transport sector and Information Technology in the frames of the project “Adaptation of 21st-century technologies for non-conventional low-emission vehicles based on composite materials”, Reg. No. NFP313010BXF3 by OPII—VA/DP/2021/9.3-01, as well as the support of the Ministry of Education, Youth, and Sports of the Czech Republic and the European Union (European Structural and Investment Funds Operational Program Research, Development, and Education) in the framework of the project “Modular platform for autonomous chassis of specialized electric vehicles for freight and equipment transportation,” Reg. No. CZ.02.1.01/0.0/0.0/16_025/0007293.

Conflicts of Interest: The authors have no relevant financial or non-financial interest to disclose.

References

- Ramanathan, A.; Krishnan, P.K.; Muraliraja, R. A review on the production of metal matrix composites through stir casting—Furnace design, properties, challenges, and research opportunities. *J. Manuf. Process.* **2019**, *42*, 213–245. [[CrossRef](#)]
- Wong, K.J.; Johar, M.; Koloor, S.S.R.; Petrú, M.; Tamin, M.N. Moisture absorption effects on mode II delamination of carbon/epoxy composites. *Polymers* **2020**, *12*, 2162. [[CrossRef](#)] [[PubMed](#)]
- Shokravi, H.; Mohammadyan-Yasouj, S.E.; Koloor, S.S.R.; Petrú, M.; Heidarrezaei, M. Effect of alumina additives on mechanical and fresh properties of self-compacting concrete: A review. *Processes* **2021**, *9*, 554. [[CrossRef](#)]
- Mohammadyan-Yasouj, S.E.; Abbastabar Ahangar, H.; Ahevani Oskoei, N.; Shokravi, H.; Rahimian Koloor, S.S.; Petrú, M. Thermal performance of alginate concrete reinforced with basalt fiber. *Crystals* **2020**, *10*, 779. [[CrossRef](#)]
- Vijayakumar, K.; Prabhu, L.; Subin, B.; Satheen, S.; Vaishnav, K. Development of Hybrid Aluminium Metal Matrix Composites for Marine Applications. In *IOP Conference Series: Materials Science and Engineering*; IOP Publishing: Bristol, UK, 2020.
- Ambali, A.O.; Bolaji, B.O.; Abdulmalik, I.O. The Processing Methods and Properties of Aluminium-SiCp Metal Matrix Composites Produced by Stir Casting for Marine Applications—A Review. *FUOYE J. Eng. Technol.* **2022**, *7*, 465–473. [[CrossRef](#)]
- Elanchezhian, C.; Ramnath, B.V.; Ramakrishnan, G.; Raghavendra, K.S.; Muralidharan, M.; Kishore, V. Review on metal matrix composites for marine applications. *Mater. Today Proc.* **2018**, *5*, 1211–1218. [[CrossRef](#)]
- Santhosh, N.; Kempaiah, U.; Gowda, A.C.; Raghu, M.; Sajjan, G. Corrosion characterization of silicon carbide and fly ash particulates dispersion strengthened aluminium 5083 composites. *J. Catal. Catal.* **2017**, *4*, 9–21.
- Koloor, S.R.; Karimzadeh, A.; Abdullah, M.; Petrú, M.; Yidris, N.; Sapuan, S.; Tamin, M. Linear-Nonlinear Stiffness Responses of Carbon Fiber-Reinforced Polymer Composite Materials and Structures: A Numerical Study. *Polymers* **2021**, *13*, 344. [[CrossRef](#)]
- Sharma, D.K.; Mahant, D.; Upadhyay, G. Manufacturing of metal matrix composites: A state of review. *Mater. Today Proc.* **2020**, *26*, 506–519. [[CrossRef](#)]
- Samal, P.; Vundavilli, P.R.; Meher, A.; Mahapatra, M.M. Recent progress in aluminum metal matrix composites: A review on processing, mechanical and wear properties. *J. Manuf. Process.* **2020**, *59*, 131–152. [[CrossRef](#)]
- Ghandvar, H.; Jabbar, M.A.; Koloor, S.S.R.; Petrú, M.; Bahador, A.; Bakar, T.A.A.; Kondoh, K. Role B4C addition on microstructure, mechanical, and Wear characteristics of Al-20% Mg2Si hybrid metal matrix composite. *Appl. Sci.* **2021**, *11*, 3047. [[CrossRef](#)]
- Foltz, J.V.; Blackmon, C.M. Metal-Matrix Composites. In *2013 ASM Handbook, Volume 2: Properties and Selection: Nonferrous Alloys and Special-Purpose Materials* ASM Handbook Committee; ASM International: Novelty, OH, USA, 2013; pp. 903–912. [[CrossRef](#)]
- Seth, P.P.; Parkash, O.; Kumar, D. Structure and mechanical behavior of in situ developed Mg 2 Si phase in magnesium and aluminum alloys—A review. *RSC Adv.* **2020**, *10*, 37327–37345. [[CrossRef](#)] [[PubMed](#)]
- Li, G.; Gill, H.; Varin, R. Magnesium silicide intermetallic alloys. *Metall. Mater. Trans. A* **1993**, *24*, 2383–2391. [[CrossRef](#)]

16. Li, C.; Wu, Y.; Li, H.; Liu, X. Morphological evolution and growth mechanism of primary Mg₂Si phase in Al–Mg₂Si alloys. *Acta Mater.* **2011**, *59*, 1058–1067. [[CrossRef](#)]
17. Qin, Q.-D.; Zhao, H.-L.; Juan, L.; Zhang, Y.-Z.; Su, X.-D. Microstructure and mechanical properties of friction stir processed Al–Mg₂Si alloys. *Trans. Nonferrous Met. Soc. China* **2020**, *30*, 2355–2368. [[CrossRef](#)]
18. Srinivas, V.; Singh, V. Development of in situ as cast Al–Mg₂Si particulate composite: Microstructure refinement and modification studies. *Trans. Indian Inst. Met.* **2012**, *65*, 759–764. [[CrossRef](#)]
19. Li, J.; Zhao, G.; Wu, S.; Huang, Z.; Lü, S.; Chen, Q.; Li, F. Preparation of hybrid particulates SiCnp and Mg₂Si reinforced Al–Cu matrix composites. *Mater. Sci. Eng. A* **2019**, *751*, 107–114. [[CrossRef](#)]
20. Moktar, M.; Ghandvar, H.; Abu Bakar, T. Microstructural and tensile properties of Al–20% Mg₂Si–xSiCp hybrid metal matrix composite. *Encycl. Renew. Sustain. Mater.* **2020**, *5*, 54–63.
21. Zulfia, A.; Putro, E.; Wahyudi, M.; Dhaneawara, D.; Utomo, B. Fabrication and characteristics of ADC-12 reinforced nano-SiC and nano-Al₂O₃ composites through stir casting route. In *IOP Conference Series: Materials Science and Engineering*; IOP Publishing: Bristol, UK, 2018.
22. Umanath, K.; Selvamani, S.; Palanikumar, K. Friction and wear behaviour of Al6061 alloy (SiCp+ Al₂O₃p) hybrid composites. *Int. J. Eng. Sci. Technol.* **2011**, *3*, 5441–5451.
23. Altinkok, N.; Coban, A. The tensile behaviour and microstructure of Al₂O₃/sicp reinforced aluminium-based mmcs produced by the stir casting method. *Int. J. Sci. Adv. Technol.* **2012**, *2*, 78–86.
24. Uvaraja, V.; Natarajan, N.; Rajendran, I.; Sivakumar, K. Tribological behavior of novel hybrid composite materials using Taguchi technique. *J. Tribol.* **2013**, *135*, 021101. [[CrossRef](#)]
25. Sharma, S.; Jagannath, K.; Prabhu, P.; Gowri, S.M.; Harisha, S.; Kini, U.A. Metallography & bulk hardness of artificially aged Al6061–B₄C–SiC stir cast hybrid composites. *Mater. Sci. Forum* **2016**, *880*, 140–143.
26. Uthayakumar, M.; Aravindan, S.; Rajkumar, K. Wear performance of Al–SiC–B₄C hybrid composites under dry sliding conditions. *Mater. Des.* **2013**, *47*, 456–464. [[CrossRef](#)]
27. Soltani, N.; Nodooshan, H.J.; Bahrami, A.; Pech-Canul, M.; Liu, W.; Wu, G. Effect of hot extrusion on wear properties of Al–15 wt.% Mg₂Si in situ metal matrix composites. *Mater. Des.* **2014**, *53*, 774–781. [[CrossRef](#)]
28. Ghorbani, M.; Emamy, M.; Nemati, N. Microstructural and mechanical characterization of Al–15% Mg₂Si composite containing chromium. *Mater. Des.* **2011**, *32*, 4262–4269. [[CrossRef](#)]
29. Abubakar, T.A. Microstructure characterization and tensile properties of Al–15% Mg₂Si–xYSZ hybrid composite. *Malays. J. Microsc.* **2019**, *15*, 1.
30. Singh, J.; Chauhan, A. Characterization of hybrid aluminum matrix composites for advanced applications—A review. *J. Mater. Res. Technol.* **2016**, *5*, 159–169. [[CrossRef](#)]
31. Zhang, J.; Fan, Z.; Wang, Y.; Zhou, B. Microstructural development of Al–15wt.% Mg₂Si in situ composite with mischmetal addition. *Mater. Sci. Eng. A* **2000**, *281*, 104–112. [[CrossRef](#)]
32. Ghandvar, H.; Farahany, S.; Idris, M.H. Effect of wettability enhancement of SiC particles on impact toughness and dry sliding wear behavior of compocasted A356/20SiCp composites. *Tribol. Trans.* **2018**, *61*, 88–99. [[CrossRef](#)]
33. Zainon, F.; Ahmad, K.R.; Daud, R. The effects of Mg₂Si (p) on microstructure and mechanical properties of AA332 composite. *Adv. Mater. Res.* **2016**, *5*, 55. [[CrossRef](#)]
34. Ghandvar, H.; Idris, M.H.; Ahmad, N.; Emamy, M. Effect of gadolinium addition on microstructural evolution and solidification characteristics of Al–15% Mg₂Si in-situ composite. *Mater. Charact.* **2018**, *135*, 57–70. [[CrossRef](#)]
35. Soltani, N.; Bahrami, A.; Pech-Canul, M.I. The effect of Ti on mechanical properties of extruded in-situ Al–15 pct Mg₂Si composite. *Metall. Mater. Trans. A* **2013**, *44*, 4366–4373. [[CrossRef](#)]
36. Ghandvar, H.; Jabbar, K.A.; Idris, M.H.; Ahmad, N.; Jahare, M.H.; Koloor, S.S.R.; Petru, M. Influence of barium addition on the formation of primary Mg₂Si crystals from Al–Mg–Si melts. *J. Mater. Res. Technol.* **2021**, *11*, 448–465. [[CrossRef](#)]
37. Khorshidi, R.; Raouf, A.H.; Emamy, M.; Campbell, J. The study of Li effect on the microstructure and tensile properties of cast Al–Mg₂Si metal matrix composite. *J. Alloys Compd.* **2011**, *509*, 9026–9033. [[CrossRef](#)]
38. Farahany, S.; Ghandvar, H.; Nordin, N.A.; Ourdjini, A.; Idris, M.H. Effect of primary and eutectic Mg₂Si crystal modifications on the mechanical properties and sliding wear behaviour of an Al–20Mg₂Si–2Cu–xBi composite. *J. Mater. Sci. Technol.* **2016**, *32*, 1083–1097. [[CrossRef](#)]
39. Archard, J. Contact and rubbing of flat surfaces. *J. Appl. Phys.* **1953**, *24*, 981–988. [[CrossRef](#)]
40. Thakur, S.K.; Dhindaw, B.K. The influence of interfacial characteristics between SiCp and Mg/Al metal matrix on wear, coefficient of friction and microhardness. *Wear* **2001**, *247*, 191–201. [[CrossRef](#)]
41. Farahany, S.; Ghandvar, H.; Bozorg, M.; Nordin, A.; Ourdjini, A.; Hamzah, E. Role of Sr on microstructure, mechanical properties, wear and corrosion behaviour of an Al–Mg₂Si–Cu in-situ composite. *Mater. Chem. Phys.* **2020**, *239*, 121954. [[CrossRef](#)]
42. Khan, M.S.; Abdul-Latif, A.; Koloor, S.S.R.; Petru, M.; Tamin, M.N. Representative cell analysis for damage-based failure model of polymer hexagonal honeycomb structure under the out-of-plane loadings. *Polymers* **2020**, *13*, 52. [[CrossRef](#)]
43. Zeng, F.-L.; Wei, Z.-L.; Li, J.-F.; Li, C.-X.; Tan, X.; Zhang, Z.; Zheng, Z.-Q. Corrosion mechanism associated with Mg₂Si and Si particles in Al–Mg–Si alloys. *Trans. Nonferrous Met. Soc. China* **2011**, *21*, 2559–2567. [[CrossRef](#)]

44. Li, C.; Sun, J.; Li, Z.; Gao, Z.; Liu, Y.; Yu, L.; Li, H. Microstructure and corrosion behavior of Al–10% Mg₂Si cast alloy after heat treatment. *Mater. Charact.* **2016**, *122*, 142–147. [[CrossRef](#)]
45. Li, Z.; Li, C.; Gao, Z.; Liu, Y.; Liu, X.; Guo, Q.; Yu, L.; Li, H. Corrosion behavior of Al–Mg₂Si alloys with/without addition of Al–P master alloy. *Mater. Charact.* **2015**, *110*, 170–174. [[CrossRef](#)]

Disclaimer/Publisher’s Note: The statements, opinions and data contained in all publications are solely those of the individual author(s) and contributor(s) and not of MDPI and/or the editor(s). MDPI and/or the editor(s) disclaim responsibility for any injury to people or property resulting from any ideas, methods, instructions or products referred to in the content.